Magnetic fields influence on sensors with electrical output under sinusoidal excitations

Nieves Medina[1], Jesús de Vicente[2], Jorge Robles[1]

[1] *Centro Español de Metrología, Calle Alfar 2, Tres Cantos, 28760 Madrid, Spain*
[2] *Escuela Técnica Superior de Ingenieros Industriales, Calle de Jose Gutierrez Abascal 2, 28006 Madrid, Spain*

ABSTRACT
This paper describes the magnetic effects studied at CEM in their realization of a primary standard for dynamic force calibration using sinusoidal excitations of force transducers, although they can also affect any sensor with an electrical output mounted on an electrodynamic shaker. In this study the electromagnetic behaviour for the interaction between sensor and shaker or a similar source of magnetic fields is explained and a solution to minimise this interaction is also included.

Corresponding author: Nieves Medina, e-mail: mnmedina@cem.minetur.es

1. INTRODUCTION

This paper describes the magnetic effects studied at CEM in their realization of a primary standard for dynamic force calibration using sinusoidal excitations of force transducers.

This work was part of a project called "Traceable dynamic measurement of mechanical quantities" financed by the European Union under the European Research Metrology Program [1].

This standard is based on the direct definition of force as mass times acceleration. The transducer is loaded with different calibrated masses and different accelerations are generated by a vibration shaker system. The acceleration is measured by a laser vibrometer traceable to the unit of length (laser wavelength).

The laser vibrometer (Polytec CLV 2534) is placed over the shaker (LDS 726 with power amplifier PA 2000, which can work from 5 Hz up to 2400 Hz) by means of a special table designed for this purpose, see Figure 1 for reference.

Being a fully dynamic measurement it requires a multichannel data acquisition system in real time. A NI PXI 1033 module with a 4462 card (24 bits, 204.8 kS/s) has been

used. The implemented software, which is programmed in Labview, samples the signals separately with a speed of 40 kS/s and applies the sine approximation method in order to
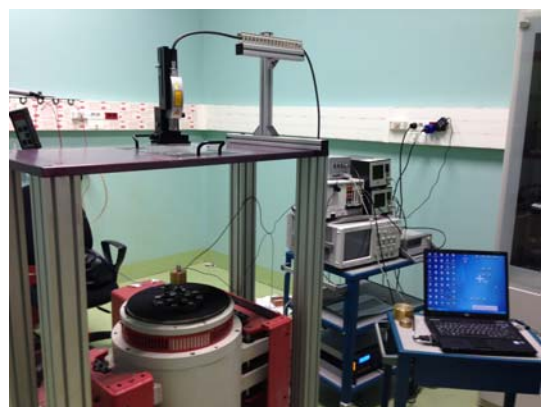

Figure 1. Overview of the standard for dynamic force calibration using sinusoidal excitations.

determine the signals amplitudes and phases in real time.

The sensor is characterised by its dynamic sensitivity, which is the ratio of its electrical output signal of the force transducer and the acting dynamic force. The sensitivity phase shift is determined as the phase difference between the sensor output and the laser vibrometer output.

The required masses for generating the forces on the sensors have been manufactured and calibrated to determine their mass and their corresponding uncertainty. The masses have nominal values 347 g, 1 kg, 2 kg, 7.3 kg and 12.3 kg. The three smaller masses are screwed to the sensor under calibration; the bigger ones are connected under pressure by means of a special adaptor. Depending on the sensor to be calibrated, special adaptors may be required in order to screw the masses to the sensor or the sensor to the shaker. Different corrections and influence factors have to be taken into account for this standard. References [2] and [3] provide complete information about this development.

2. DESCRIPTION

The parameter that characterises the force transducer is the sensitivity S, which is defined as the ratio of the electrical output signal of the transducer to the acting dynamic force. Its module can be determined as

$$S = \frac{U/V}{(m + m_i) \cdot a} \, , \tag{1}$$

where U is the output of the conditioning amplifier, V is the amplification factor of the conditioning amplifier, m is the mass for loading the transducer, m_i is the internal mass of the transducer that contributes as a load and a is the acceleration measured by the laser vibrometer.

The sensitivity phase is determined as the phase difference between the sensor output and the laser vibrometer output. The possible effect on the phase of the conditioning amplifier is considered negligible.

This work arises from the study of the behaviour of the sensor sensitivity at low frequencies. In principle, the lower the frequency the behaviour should be increasingly closer to the static behaviour, that is, the sensor sensitivity must remain constant. This sensitivity behaviour is as expected for heavy loads, but not for small loads. In fact, the smaller the load, the sensitivity variation increases.

In this work the sensitivity behaviour has been studied in the range from 5 Hz to 200 Hz. This study was conducted for different excitation accelerations according to the possibilities of the vibration shaker and for several sensors with different size and working principle, resistive or piezoelectric. Figure 2 to Figure 6 are examples of this kind of behaviour for different sensors with two different working principles. There is no effect on the phase shift for the piezoelectric sensor, so no plot is shown.

The expanded uncertainty estimation is 0.5 % for the sensitivity modulus divided by the sensitivity modulus for 200 Hz and 0.5º for the sensitivity phase shift.

The results of this study can be summarised as follows.

The first issue that has to be remarked is the fact that these effects are not dependent on the acceleration. They do not depend on either its magnitude or the chosen reference to measure it, because the same results were obtained using the laser vibrometer or a reference accelerometer. They only appear for low frequencies, typically less than 40 Hz.
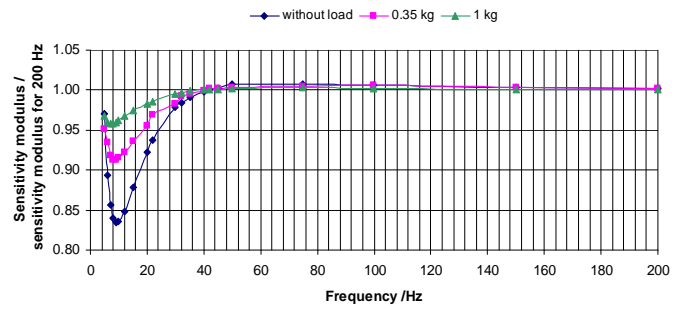
Figure 2. Plot showing the sensitivity modulus divided by the sensitivity modulus for 200 Hz versus excitation frequency for the INTERFACE 1610 sensor (resistive sensor) for the cases: without load, 0.35 kg and 1 kg.
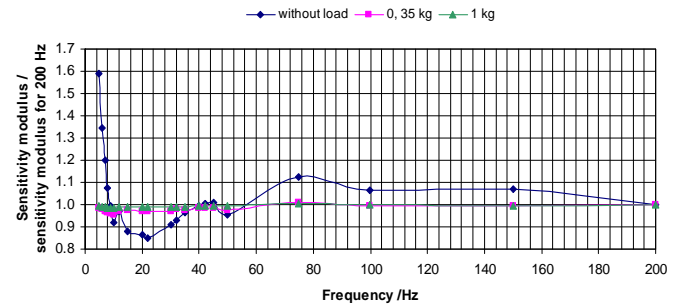
Figure 3. Plot showing the sensitivity modulus divided by the sensitivity modulus for 200 Hz versus excitation frequency for the HBM U2B sensor (resistive sensor) for the cases: without load, 0.35 kg and 1 kg.
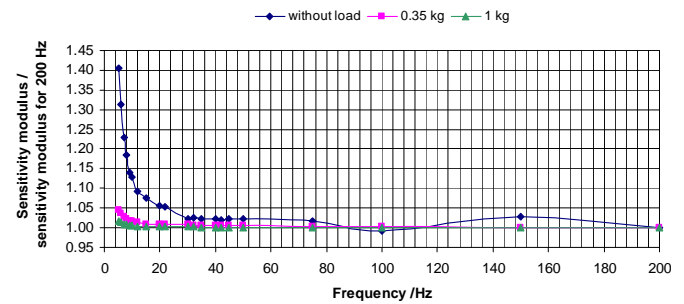
Figure 4. Plot showing the sensitivity modulus divided by the sensitivity modulus for 200 Hz versus excitation frequency for the KISTLER 9175B sensor (piezoelectric sensor) for the cases: without load, 0.35 kg and 1 kg.
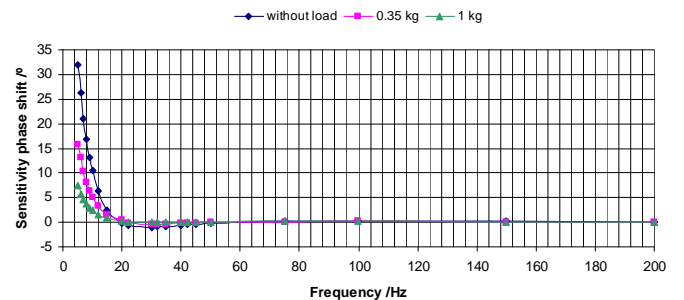
Figure 5. Plot showing the sensitivity phase shift versus excitation frequency for the INTERFACE 1610 sensor (resistive sensor) for the cases: without load, 0.35 kg and 1 kg.

There is a case, the HBM U9B sensor, which is a resistive sensor, where this effect does not occur. The only difference that distinguishes it from the other tested resistive sensors is its small size, so it is clear that size may have an influence.

These effects increase as the load decreases. In fact it is more important when the sensor is not loaded.
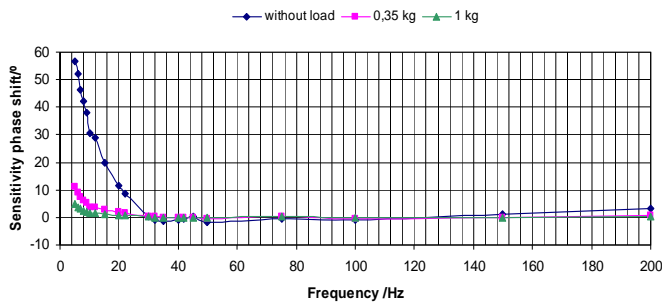
Figure 6. Plot showing the sensitivity phase shift versus excitation frequency for the HBM U2B sensor (resistive sensor) for the cases: without load, 0.35 kg and 1 kg.

The fact that these effects are not dependent on the acceleration and how it is measured, decrease with excitation frequency and load and decrease with the sensor size, indicates that they cannot be dynamic effects such as rocking motion or resonances. It is therefore thought that an interaction between sensor and vibration shaker may be a possible explanation for these effects. The operation principle of the electrodynamic shaker (the armature moves because of the Lorentz force) makes magnetic fields presence necessary for its operation, so a kind of magnetic effect is thought to be a good candidate for a possible explanation.

3. UNDERSTANDING THE EFFECTS

As a first step the magnetic field in contact with the centre of the shaker armature (where the sensor is connected) was measured obtaining a value of 2.3 mT. At this same position but 15 cm higher the magnetic field is less than 0.5 mT. These fields are relatively small and are within the specifications of the shaker itself.

In order to check whether the observed effects are actually caused by magnetic fields, a large magnetic field generated by a large permanent magnet was put close to the sensor. The intention is to magnify these effects by the presence of the magnet.

As a first attempt the magnet was near the sensor and the sensor was connected to the shaker. Sensor tests were then performed in the range from 5 Hz to 200 Hz with the sensor moving and the magnet hanging in a stationary position. These tests were carried out at several distances, different accelerations and always with the sensors unloaded, so that their output could only be influenced by magnetic effects. As a result no different effects from the ones that had already been observed could be seen.

In the second attempt (Figure 7) it was decided to reverse the sensor-magnet configuration and connect the magnet to the shaker, so it moves with it, and leave the sensor hanging to remain static. With this new configuration the effects presented from Figure 8 to Figure 18 were obtained.

These results were completely unexpected because an unloaded sensor in a static position should have a constant output (zero output) that should not depend on other external factors. On the contrary, these results show a clear dependency on excitation frequency: for the resistive sensors as the inverse of the frequency (Figure 12, Figure 13 and Figure 14) and for the piezoelectric sensor as the inverse of the frequency squared (Figure 15). For the HBM U9B sensor this effect is much smaller and there is only a clear influence for frequencies less
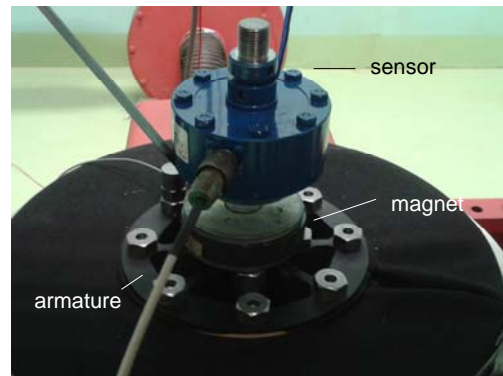

Figure 7. Photograph showing the sensor-magnet configuration in the second attempt: the sensor is hanging, without any acting force on it, and the magnet is moving sinusoidally versus time as it is attached to the shaker.
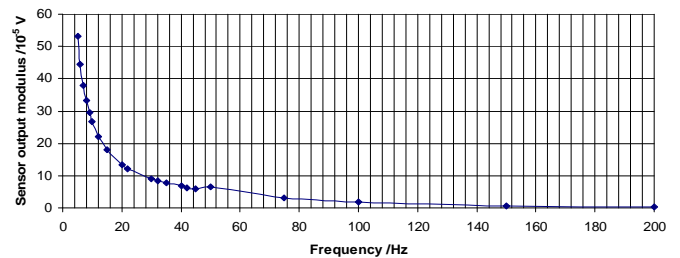

Figure. 8. Plot showing sensor output modulus versus excitation frequency for INTERFACE 1610 sensor (resistive sensor).
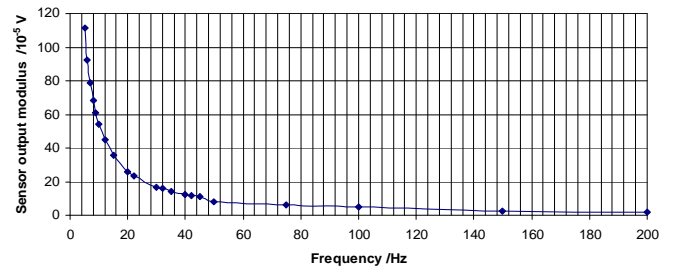

Figure 9. Plot showing sensor output modulus versus excitation frequency for HBM U2B sensor (resistive sensor).
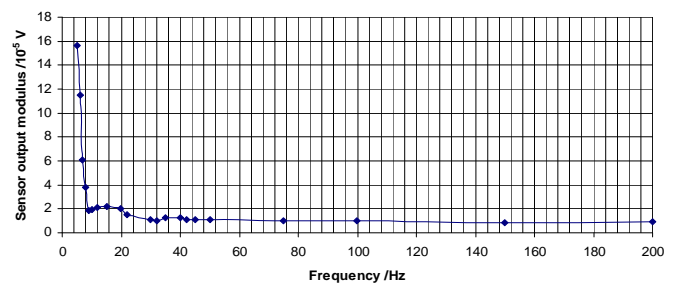

Figure 10. Plot showing sensor output modulus versus excitation frequency for HBM U9B sensor (resistive sensor).

than 10 Hz (Figure 14). It was also obtained that for frequencies more than 200 Hz no effect was observed.

According to Figure 16, Figure 17 and Figure 18 it can be deduced that the sensor's output phase shift is -90° for resistive sensors and 0° for piezoelectric sensors ($\pm$ 180°, due to the indeterminacy of the arc tangent function used for calculating the phase). The effect on the phase shift for the HBM U9B sensor is negligible, so no plot is shown.
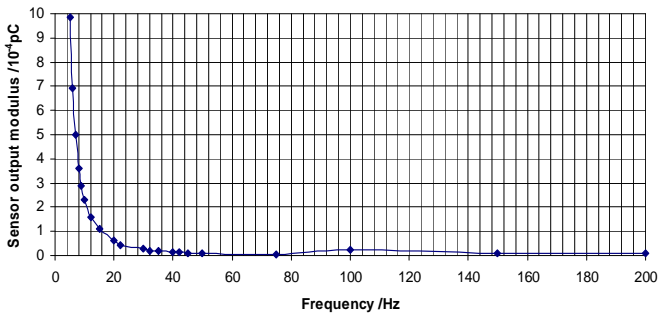
Figure 11. Plot showing sensor output modulus versus excitation frequency for KISTLER 9175B sensor (piezoelectric sensor).
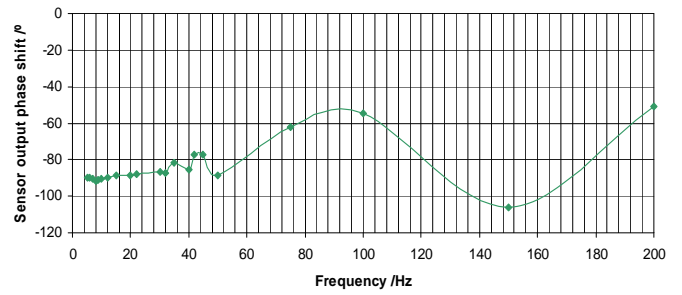

Figure 12. Plot showing sensor output modulus versus the inverse of the frequency for INTERFACE 1610 sensor (resistive sensor).

Figure 13. Plot showing sensor output modulus versus the inverse of the frequency for HBM U2B sensor (resistive sensor).

Figure 14. Plot showing sensor output modulus versus the inverse of the frequency for HBM U9B sensor (resistive sensor).

Figure 15. Plot showing sensor output modulus versus the inverse of the frequency squared for KISTLER 9175B sensor (piezoelectric sensor).

Figure 16. Plot showing sensor output phase shift versus the frequency for INTERFACE 1610 sensor (resistive sensor).
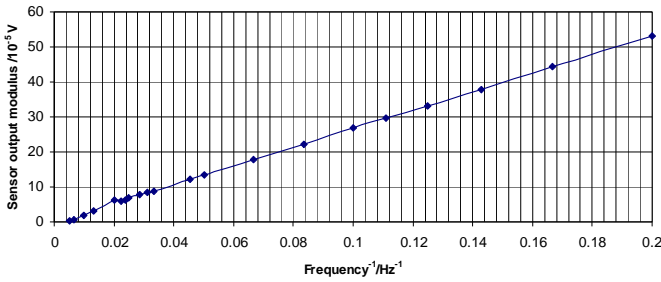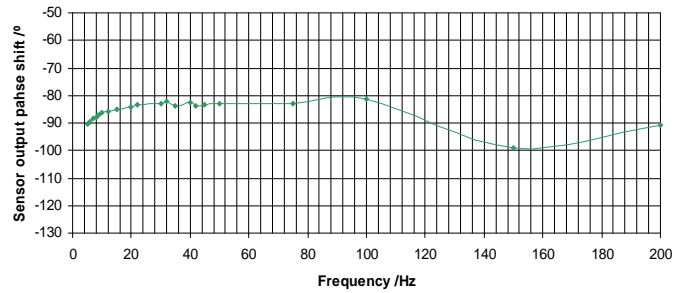

Figure 17. Plot showing sensor output phase shift versus the frequency for HBM U2B sensor (resistive sensor).
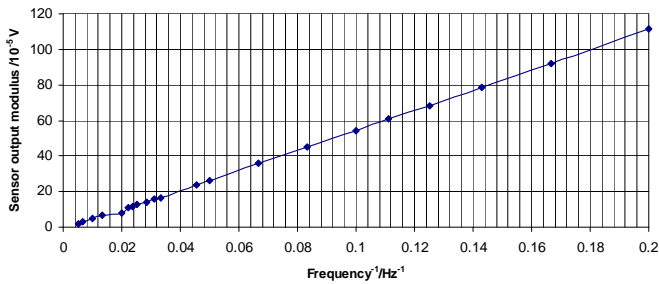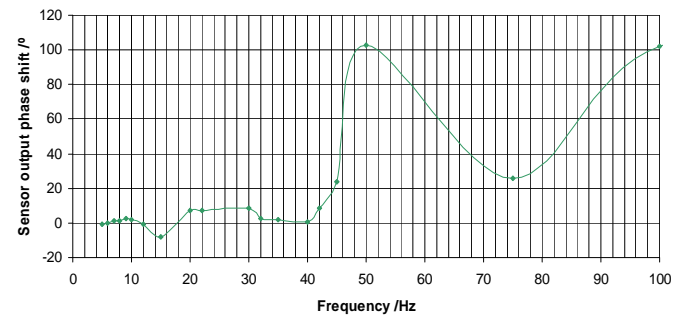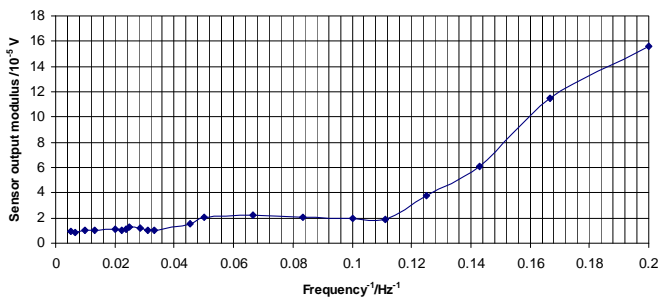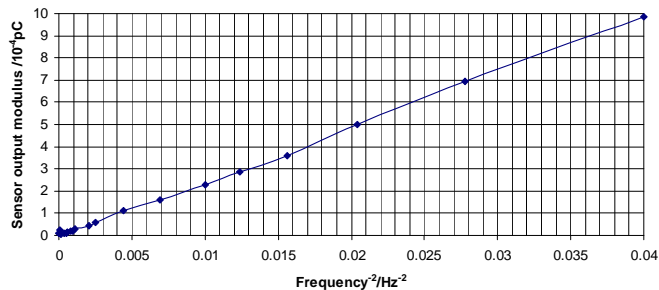

Figure 18. Plot showing sensor output phase shift versus the frequency for KISTLER 9175B sensor (piezoelectric sensor).

These measurements are more reliable at low frequencies, where the results are closer to constant values; but generally these constant values can be extrapolated to the entire measurement range, as their measurement errors are related to the fact that the sensor's output amplitude will be much lower as the excitation frequency increases.

The conclusion from these experiments is that very similar effects as the ones previously observed were obtained, but magnified. This is due to the high intensity of the magnetic field generated by the moving magnet; but the most important achievement has been to prove that these effects were caused by a magnetic field whose intensity close to the sensor varies sinusoidally with time. In this case the distance between the moving magnet and the sensor varies sinusoidally with time and, therefore, the magnetic field intensity generated close to the sensor varies accordingly.

4. THEORETICAL JUSTIFICATION

The operating principle of the electrodynamic shaker, in order to achieve a sinusoidal motion of its armature, is based in the Lorentz force law. A coil with N turns with length l and a current I passing through, which varies sinusoidally with

excitation frequency ω, is attached to the shaker armature. This coil is immersed within a static magnetic field with magnetic flux density B. This is necessary so that the armature can move according to the Lorentz force law:

$$\boldsymbol{F} e^{j\omega t} = NI\boldsymbol{I} e^{j\omega t} \times \boldsymbol{B}. \tag{2}$$

The magnetic flux density B is generated by another coil with a direct current passing through it. There is another coil called "degauss" coil that counteracts the effects of B in the environment. These magnetic fields are static and have no effect on the measurement.

The frequency dependent magnetic field that could explain these effects comes from the current $I(\omega)$, which passes through the coil. This magnetic field $\boldsymbol{B}'(\omega)$ will vary with the excitation frequency and comes from the application of Biot and Savart law [4]:

$$\boldsymbol{B}' e^{j\omega t} = \frac{\mu_0}{4\pi} NI e^{j\omega t} \oint \frac{d\boldsymbol{l} \times \boldsymbol{u}_r}{r^2}, \tag{3}$$

where r is the distance between the coil and the place where the magnetic flux density is evaluated and $\boldsymbol{l}$ is the length of each turn.

Using cylindrical coordinates (r, z, φ) $\boldsymbol{I}$ will only have one component I_φ, so the magnetic field $\boldsymbol{B}'$ can only have two components B'_z and B'_r. The effect of this sinusoidal magnetic field produces a current density $\boldsymbol{J}'(\omega)$ at the same time, which also varies sinusoidally, see Figure 19.

If the medium that generates this output can be assumed as isotropic and homogeneous as a first approximation, Maxwell equations can be applied as follows [5], where the medium is considered to have permeability μ and conductivity σ and the fields variation with time is sinusoidal with frequency ω,

$$\begin{aligned}\nabla \times \boldsymbol{J}' &= -j\omega\sigma\boldsymbol{B}' \\ \nabla \times \boldsymbol{B}' &= \mu\boldsymbol{J}'\end{aligned}. \tag{4}$$

The solution for this system of equations is rather complex. The current density $\boldsymbol{J}'$ will only have one component, J'_φ, as $\boldsymbol{B}'$ has two components, B'_z and B'_r. This solution is given by (5),

$$J'_\varphi(r, z) = K \exp\left\{-\left(j\alpha\omega\sigma\mu\right)^{1/2} z\right\} \cdot J_1\left\{\left(j(\alpha-1)\omega\sigma\mu\right)^{1/2} r\right\} \tag{5}$$

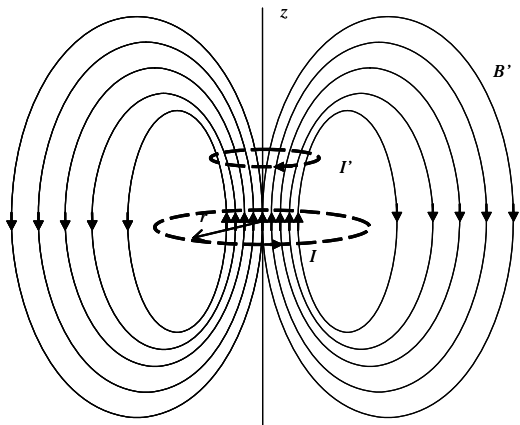where J_1 is the Bessel function for first kind, and K and α are constants. In order to obtain this solution it has been taken into account that, as long as the sensor is far from the source of the electromagnetic field (either z or r increase) the induced current density should become zero. It is also required that $\alpha > 1$ in order to avoid divergent solutions.

As a consequence, the induced current will have one single component along the φ direction and its module will be given as the solution for (6),

$$I'_\varphi = \int J'_\varphi \cdot dS. \tag{6}$$

The solution for the previous integral is given by the following expression (7),

$$I'_\varphi = \frac{K \cdot \exp\left\{-\left(j\alpha\omega\sigma\mu\right)^{1/2} z\right\} \cdot J_0\left\{\left(j(\alpha-1)\omega\sigma\mu\right)^{1/2} r\right\}}{j\sqrt{\alpha(\alpha-1)}\omega\sigma\mu}. \tag{7}$$

This solution applies to each surface element of the medium that generates the sensor output. It is obvious then that the induced current will depend on this medium size.

In order to study the modulus behaviour of the induced current I'_φ as a function of the excitation frequency ω, the function $y(x)$ has been studied. It is defined according to (8):

$$y(x) = \frac{e^{-x^{1/2}} \cdot J_0\left(x^{1/2}\right)}{x}. \tag{8}$$

The plots for this function versus x and $1/x$ are given in Figure 20 and Figure 21, respectively.

For Figure 20 it is clear that the same behaviour is observed as in Figure 8, Figure 9, Figure 10 and Figure 11.

For Figure 21 it is also clear that the observed behaviour is the same as in Figure 12, Figure 13, Figure 14 and Figure 15. Firstly the function value is zero but as $1/x$ increases (or x decreases) there is a clear linear dependency. As a consequence and for practical purposes, for excitation frequencies where an effect is observed, the dependency in (9) is expected,

$$I'_\varphi \propto \frac{1}{j\omega}. \tag{9}$$

Figure 20. Plot of $y(x)$ versus x.
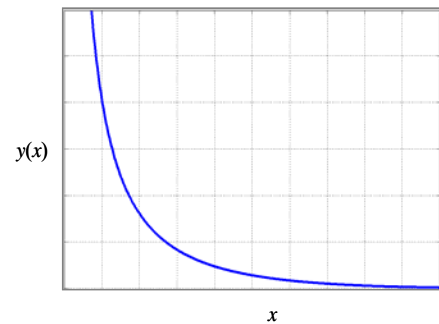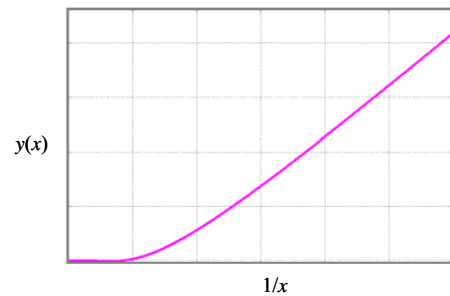

Figure 21. Plot of $y(x)$ versus $1/x$.

Figure 19. Schematic diagram showing the current I that passes through a turn of the shaker coil, the magnetic field lines for B' and the subsequent induced current I' in the sensor.

The result shown in (9) is very important and it is indeed what explains the observed effects. The induced current modulus is proportional to the inverse of the excitation frequency and its phase shift is -90°. As it applies to each surface element of the medium that generates the sensor output, it also explains why this effect depends on its size.

Most force sensors comprise an elastic element that deflects with the force and a sensing element fixed to the elastic element, which is deformed as the elastic element deflects. The sensing element in the case of a resistive sensor consists of four strain gauges in a Wheatstone bridge configuration. It measures the deformation (strain) as a change in electrical resistance, which is a measure of the strain and hence the applied force. The strain gauges and their corresponding electrical connections are electrically isolated from the elastic element and they are the media that generates the sensor output, so the output will depend directly on their size. In most cases resistive sensors with the same type but different capacity only differ on the size of the elastic element, so the expected effect will be the same for any of them.

The result shown in (9) is clearly what was obtained when the magnet was connected to the shaker and the sensor was hanging freely over it. Although, when only the shaker is considered, the generated magnetic field is smaller and the sensor sensitivity dependency with the inverse of the excitation frequency may not be so clear. On the other hand, the strain gauges that generate the sensor output may not fulfil homogeneous and isotropic conditions in full.

All of the previous statements make sense for resistive sensors. Since their impedance is basically resistive, their output will be directly proportional to the induced current. In the case of piezoelectric sensors, the observed output depends on the inverse of the frequency squared. This case is also justified because these sensors direct outputs are not currents but charges. In general, the charge Q that is generated by a sinusoidal current I with amplitude I_0 is given by (10):

$$Q = \int I \, dt = \int I_0 e^{j\omega t} dt = \frac{I}{j\omega}. \tag{10}$$

This result indicates that the charge generated by the current induced by the sinusoidal magnetic field is itself inversely proportional to frequency and with a -90° phase shift. Moreover, it must be pointed out that, in the current use of the sensor with load and no influence of non static magnetic fields, currents are never generated and only charges which are proportional to the force are generated. As a consequence, this dependency with frequency and this -90° additional phase shift are never observed. Another way to express this fact is to say that the piezoelectric impedance is basically capacitive ($Z = 1/j\omega C$).

Therefore, if the current induced by the non static magnetic effects depends on the inverse of the excitation frequency with a -90° additional phase shift, the output voltage induced by this effect in a piezoelectric sensor will show a dependency as the inverse of the excitation frequency squared and a 180° total phase shift (or 0° due to the indeterminacy of the arc tangent function used for determining the phase shift).

The sensing element in the case of piezoelectric sensors is a piezoelectric material. Piezoelectric materials have very low conductivity, so it is very unlikely these materials may generate the electrical output under study. However there will be elements such as electrical connections and plates, which will be in touch with the piezoelectric material, and are made of

conductive metals or alloys. These elements will be the media where the current will be induced.

5. MINIMIZING THE EFFECTS

As a consequence of the dependency with the distance to the source of the electromagnetic fields provided by (7) and in order to minimise these magnetic effects, a special coupler has been used to increase the connection distance between sensor and shaker armature with excellent results (Figure 22).

As a general result, a sufficient increase in the distance between the sensor and the shaker armature will avoid the problem. In order to determine this sufficient increase expression (11) is evaluated. This expression has been directly obtained from (7).

$$\frac{I'_\varphi(z = L_2)}{I'_\varphi(z = L_1)} = \exp\left\{-\left(j\alpha\omega\sigma\mu\right)^{1/2}\left(L_2 - L_1\right)\right\}. \tag{11}$$

In principle the required increase in the distance $L_2 - L_1$ can be easily deduced from (11). α is an unknown constant, which has to satisfy $\alpha > 1$. In order to obtain this sufficient increase in the distance, the worst case can be assumed, that is $\alpha \approx 1$. The worst case can also be assumed for the permeability μ. As a consequence the assumed relative permeability will be $\mu_r \approx 1$. The only cases where it will be very different from 1 are the cases of ferromagnetic materials, where $\mu_r >> 1$ but, as the worst case is assumed, the previous assumption is justified. The main problem is to determine the conductivity, as no information is easily found about the sensor materials and the conductivity of metal alloys can differ from 7×10^7 S/m to 6×10^5 S/m. Obviously the excitation frequency ω to be considered will be the lowest of the shaker working range.

In order to determine an appropriate length for the coupler the following considerations have been taken into account. The lowest excitation frequency to be considered is 5 Hz, as it is the limit for the shaker. There was no information available about the materials that could be part of the sensing element for the sensors under study, so some assumptions were made. In the case of the resistive sensors constantan (45 % Ni, 55 % Cu) with 2×10^6 S/m could be assumed as being a typical material for strain gauges. In the case of the piezoelectric sensor the
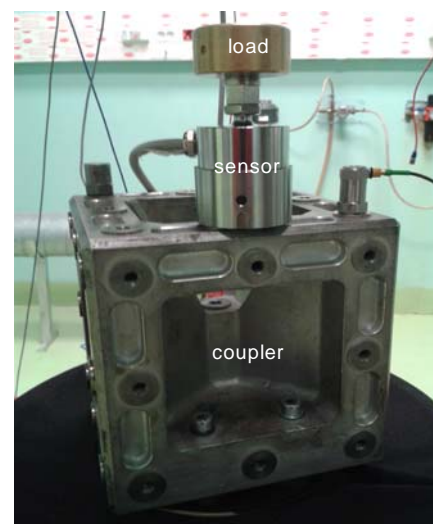

Figure 22. Photograph showing the measurement configuration when the coupler is used to minimise the magnetic effects.

assumed material was steel, so an approximate conductivity of 1.3×10^6 S/m can be assumed as the worst case. This value is lower than the one assumed for the resistive sensors, so it will be assumed as the worst case value.

Figure 23 shows the decrease of these effects versus the increase in the distance to the source of the magnetic fields as a result of (11). For an increase in the distance of 10 cm the decrease in the effect is 98 %. The coupler used in this work is 17 cm high. For this increase in the distance a 99.9 % decrease in the magnetic effects is expected.

This result agrees completely with the experimental results shown in Figure 24 to Figure 28. They show the effects on sensitivity modulus and phase shift when using this coupler compared to not using it in the case of no load, where the influence of a non static magnetic field is maximum.

This coupler, however, may have the disadvantage of magnifying the effects of transversal acceleration and resonances, which increase with excitation frequency. As a consequence, the coupler should be used only at low frequencies and it is recommended the sensor to be coupled directly to the exciter at higher frequencies.

Figure 23. Plot showing the decrease of the magnetic effects versus the increase in the distance to the source of the electromagnetic fields as a function of expression (11).
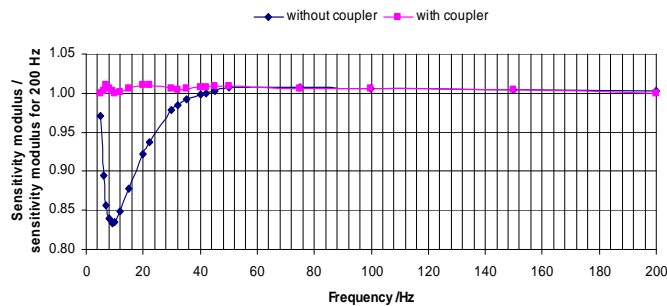

Figure 24. Plot showing the sensitivity modulus divided by the sensitivity modulus for 200 Hz versus frequency for the INTERFACE 1610 sensor (resistive) without load for the cases: with or without coupler.
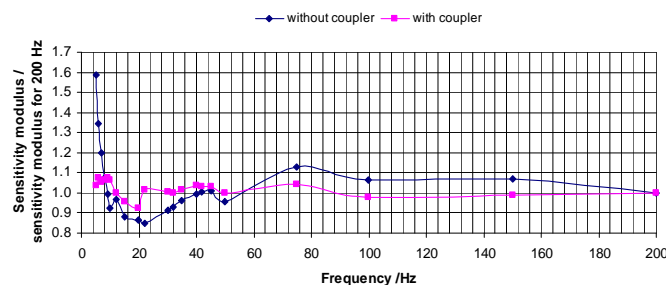

Figure 25. Plot showing the sensitivity modulus divided by the sensitivity modulus for 200 Hz versus frequency for the HBM U2B sensor (resistive) without load for the cases: with or without coupler.
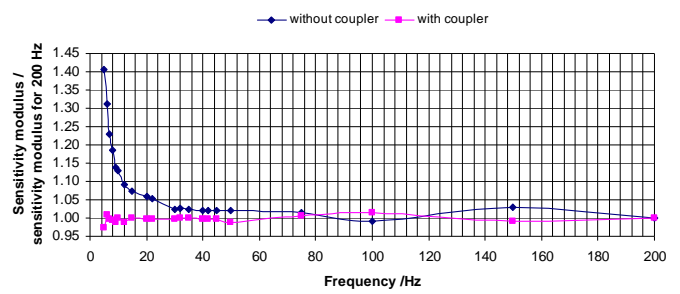

Figure 26. Plot showing the sensitivity modulus divided by the sensitivity modulus for 200 Hz versus frequency for the KISTLER 9175B sensor (piezoelectric) without load for the cases: with or without coupler.
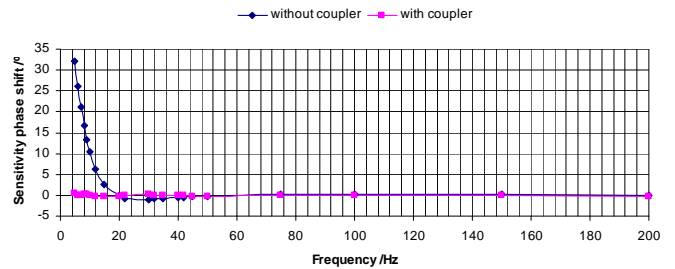

Figure 27. Plot showing the sensitivity phase shift versus frequency for the INTERFACE 1610 sensor (resistive) without load for the cases: with or without coupler.
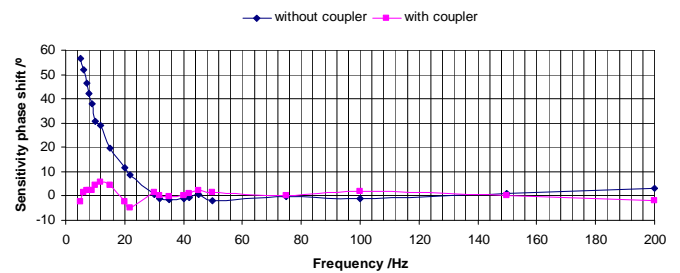

Figure 28. Plot showing the sensitivity phase shift versus frequency for the HBM U2B sensor (resistive) without load for the cases: with or without coupler.

6. CONCLUSIONS

In this paper the magnetic effects caused by a non static magnetic field on sensors with electrical output have been described and fully explained. The sensors under study have been piezoelectric and resistive force sensors and the non static magnetic field has been generated by an electrodynamic vibration shaker.

It has been discovered that these effects are more important the lower the excitation frequency and the sensor load are, but they usually increase with the sensor size.

The magnitude of the magnetic effects discovered for force sensors in this study is very important. In the current use of accelerometers with electrodynamic shakers some similar behaviour could be expected, but it may not be so important because the accelerometer size is generally smaller as well as the current that passes through the shaker armature coil used in accelerometer calibrations.

On the other hand, a sufficient vertical distance between sensor and armature, which could be achieved increasing the coupler length, assures that these effects could be negligible independently of the sensor size.

REFERENCES

[1] C. Bartoli et al. "Traceable dynamic measurement of mechanical quantities: objectives and first results of this European project", XX IMEKO World Congress, Pattaya, Thailand, 2012, https://www.imeko.org/publications/wc-2012/IMEKO-WC-2012-TC21-O7.pdf.

[2] N. Medina, J. Robles, J. de Vicente, "Realization of sinusoidal forces at CEM", IMEKO 22nd TC3, 15th TC5 and 3rd TC22 International Conferences, Cape Town, South Africa, February 2014, https://www.imeko.org/publications/tc22-2014/IMEKO-TC3-TC22-2014-001.pdf.

[3] N. Medina, J. de Vicente, "Force Sensor Characterization Under Sinusoidal Excitations", Sensors 2014, 14(10), p 18454-18473.

[4] W. R. Smythe, Static and dynamic electricity, McGraw-Hill, New York, 1950.

[5] Z. Popovic, et al, Introductory Electromagnetics, 1ª ed. Prentice Hall, 2000.